Journal of Electron Microscopy **50(4)**: 311–319 (2001)

Letter

The structure of Si nanocrystals on SiC

Ute Kaiser[1,*], Andrey Chuvilin[2] Koh Saitoh[3] and Wolfgang Richter[1]

[1]Institut für Festkörperphysik, Friedrich-Schiller Universität, D-07743 Jena, Germany and [2]Institute for Catalysis, Novosibirsk 90630090, Russia, [3]Research Institute for Scientific Measurements, Tohoku University, Sendai 980-8577
[*]To whom correspondence should be addressed. E-mail: kaiser@pinet.uni-jena.de

Abstract Si nanocrystals grown on cubic SiC have been characterized using high-resolution transmission electron microscopy. At lower temperatures nanocrystals grow in two different orientations, whereas at higher temperatures they grow in a single preferred orientation. The nanocrystals are shown to be unstrained; in some cases possibly due to the presence of a thin amorphous wetting layer.

Keywords high-resolution TEM, molecular beam epitaxy, strain analysis, Si nanocrystals, SiC

Received 10 April 2001, accepted 24 May 2001

The strain-induced self-assembly of islands in heteroepitaxial systems, followed by lateral overgrowth, is of interest for the fabrication of novel optoelectronic devices [1]. As SiC is a wide band-gap material, the Si-SiC system shows a large conduction band discontinuity that favours interband optics [2]. If Si nanocrystals are to show quantum size effects they must be both 2 to 5 nm in size and strained [3]. Molecular beam epitaxy (MBE) can be used to fabricate such nanostructures [4], and their growth can be monitored *in situ* using reflection high-energy electron diffraction. Si nanocrystals have been reported on cubic SiC grown by MBE [5], however, neither their defect state nor their strain state has been characterized. Nanocrystal formation is known to proceed by a Stranski-Krastanov mode, whereby 3-D islands assemble after a few monolayers of 2-D growth. In systems that exhibit a misfit of below 10%, this 2-D layer accommodates a large part of the strain [6] and results in a critical thickness for dislocation introduction [7]. In the Si-SiC system the misfit is much larger (25%), and the critical thickness and island density are more likely to be determined by the deposition conditions [5].

Strain determination from high-resolution transmission electron microscope (HRTEM) images typically requires the comparison of experimental data with simulations [8]. Care is required because lattice fringe spacings may be affected by the aberrations of the microscope [9] as well as by crystal tilt, thin foil relaxation [10] and local sample thickness variations [11]. In the present work, Si nanocrystals were grown by MBE (at 500°C) onto as-grown 3C-SiC and after 3C-SiC layer deposition at near equilibrium conditions (>900°C). Details of the MBE growth are described elsewhere [5]. Cross-sectional samples were prepared for transmission electron microscopy (TEM) using mechanical polishing, dimpling and low-angle Ar-ion milling. Nanocrystals were examined using a JEOL-3010 TEM, which is equipped with a LaB_6 cathode and a slow-scan CCD camera and has a point resolution of 0.21 nm. Lattice fringe spacings were measured using Diffpack and NCEM plug-ins for Digital Micrograph [12].

Figure 1a shows a cross-sectional image of a cubic SiC layer that contains a number of facets and stacking faults on which Si nanocrystals form preferentially. The Si dots can hardly be revealed at this magnification. (The black arrow points to the Si dot seen in Fig. 1c in higher magnification.) Extrinsic stacking faults in SiC are found to continue into Si (Fig. 1b, see the black arrow), and several stacking faults form in the nanocrystals when the substrate surface is inclined (Fig. 1c). Although strain in the Si is relieved by such defects [13], light emission may not then occur due to defect recombination. Following low temperature growth (500°C), the Si crystals exhibit two orientation relationships with equal probabilities, as shown in Fig. 2. Dot type I (Fig. 2a) corresponds to (111)SiC // (220)Si and (11-2)SiC // (002)Si, while dot type II (Fig. 2b) corresponds to (111)SiC // (111)Si and (11-2)SiC // (11-2)Si. In both dot types the misfit with the substrate along $[\text{-}1\text{-}12]_{SiC}$ is 25%. Along $[1\text{-}10]_{SiC}$ the misfit is 1.6% for type I and 25% for type II. Figures 3 and 4 show examples of the two dot types, alongside Fourier transforms calculated from the images. In Fig. 4 the substrate and the dot are in a twin orientation relationship. Type I and II dots typically form as pyramids and truncated pyramids, respectively. Local strain analysis was performed from the HR images. Grey-scale images of two components of the strain matrix [8], e_{xx} (Figs 5b and 5e) and e_{yy} (Figs 5c and 5f), are shown below the corresponding HR

images (Figs 5a and 5d). The uniformity of the maps of e_{xx} (Figs 5b and 5e) shows that no strain is present in this direction. In contrast, e_{yy} shows a variation parallel to the interface, which is seen in Fig. 5c and is most pronounced in Fig. 5f, as indicated by the white arrows. This variation is located at the position of the amorphous layer on the substrate surface and cannot be attributed to lattice parameter changes. In addition, convergent beam electron diffraction patterns have been obtained from dots of both dot types and their underlying substrate. As all dots studied were below 800 Å thick in beam direction, no sharp intensities in the CBED discs are seen. Therefore, the disc positions only could be used for lattice parameter measurements. No strain in the dot or matrix could be measured. The lack of strain in the dots may be explained by the presence of a thin amorphous Si wetting layer (Figs 5a and 5d). The thin foil surface relaxation [14] can be discounted as the matrix is rather thick.

For growth near equilibrium conditions (>900°C), small (<20 nm) dots of type I that are elongated along [11-2] are observed (Fig. 1b) in contrast to the dot shape at lower temperature (Figs 3a and 4a). The shape transition at low and high temperature growth will be a matter of further investigations. No amorphous layer is present at the substrate-dot interface. In defect-free dots (Fig. 6a), strain analysis shows significant negative e_{yy} values near the substrate-dot interface (Fig. 6c). Simulations performed for a matrix that is much thicker than the dot (Figs 7d–f) show only little variation in e_{xx} (Fig. 7e) and e_{yy} (Fig. 7f). However, if the dot and the matrix are now tilted by 2 mrad (0.1°) parallel to the interface, as shown in Figs 7g–i, good qualitative agreement is obtained with the experimental data, highlighting the fact that measured variations in lattice fringe spacing may originate from small crystal tilts rather than from strain. A systematic analysis of the data did not provide convincing evidence for the presence of measurable strains in any of the nanocrystals examined, despite the absence of an amorphous wetting layer. However, it should be noted that the effect of the possible contraction of the dot in the direction of high misfit perpendicular to the interface (see the [11-2] projection in the scheme (Fig. 2)) might cause similar contrast changes. This effect is currently under calculation on the base of molecular dynamics and will be reported in due cause.

Acknowledgements

This work was supported by the Sonderforschungsbereich 196. The authors acknowledge Dr Andreas Fissel for the MBE growth.

References

1 Ross F M, Tersoff J, and Tromp R M (1998) Coarsening of self-assembled Ge quantum dots on Si(001). *Phys. Rev. Lett.* **80**: 984–987.

2 Pavebi L, DalNegro L, Mozzoleni C, Franco G, and Priolo F (2000) Optical gain in Si nanocrystals. *Nature* **408**: 440–445.

3 Takagahara T and Takeda K (1992) The theory of quantum confinement effect on excitons in quantum dots of indirect-gap materials. *Phys. Rev. B* **46**: 15578–15585.

4 Fissel A, Schröter B, Kaiser U, and Richter W (2000) Advances in the molecular-beam epitaxial growth of artificially layered heteropolytypic structures of SiC. *Appl. Phys. Lett.* **77**: 2418–2420.

5 Fissel A, Akhtariev R, Kaiser U, and Richter W (2001) MBE growth of Si on SiC(0001): from superstructures to islands. *J. Crystal Growth* (accepted).

6 Tillmann K, Thust A, Lentzen M, Swiatek P, Förster A, Urban K, Laufs W, Gerthsen D, Remmle T, and Rosenhauer A (1996) Determination of segregation, elastic strain and thin-foil relaxation in $In_xGa_{1-x}As$ islands on GaAs (001) by high-resolution transmission electron microscopy. *Philos. Mag. Lett.* **74**: 309–315.

7 Christiansen S, Albrecht M, Michler J, Strunk H P, Hansson P D, and Bauser E (1995) Reduced effective misfit in laterally limited structures such as epitaxial islands. *Appl. Phys. Lett.* **66**: 574–576.

8 Hÿtch M J, Snoeck E, and Kilaas R (1998) Quantitative measurement of displacement and strain fields from HREM micrographs. *Ultramicroscopy* **74**: 131–146.

9 Saxton W O, Dürr R, and Baumeister W (1992) *Ultramicroscopy* **46**: 287–297.

10 Tillmann K, Lentzen M, and Rosenfeld R (1999) Impact of strain relaxation induced local crystal tilts on the quantitative evaluation of microstructure by high-resolution transmission electron microscopy. *Inst. Phys. Conf. Ser.* **164**: 15–22.

11 Plamann T, Hÿtch M J, Kret S, and Laval J Y (1999) Strain mapping in semiconductor heterostructures using HREM. *Inst. Phys. Conf. Ser.* **164**: 23–26.

12 *User Manual for Digital Micrograph* (Gatan, Inc., Pleasanton, CA).

13 Jin-Phillipp N Y and Phillipp F (1999) Defect formation in self-assembling quantum dots of InGaAs on GaAs: a case study of direct measurements of local strain from HREM. *J. Microsc.* **194**: 161–170

14 Treacy M M J and Gibson J M (1986), The effect of elastic relaxation on transmission electron microscopy studies of thinned composition modulated materials. *J. Vac. Sci. Technol.* **B4**: 1458–1466.

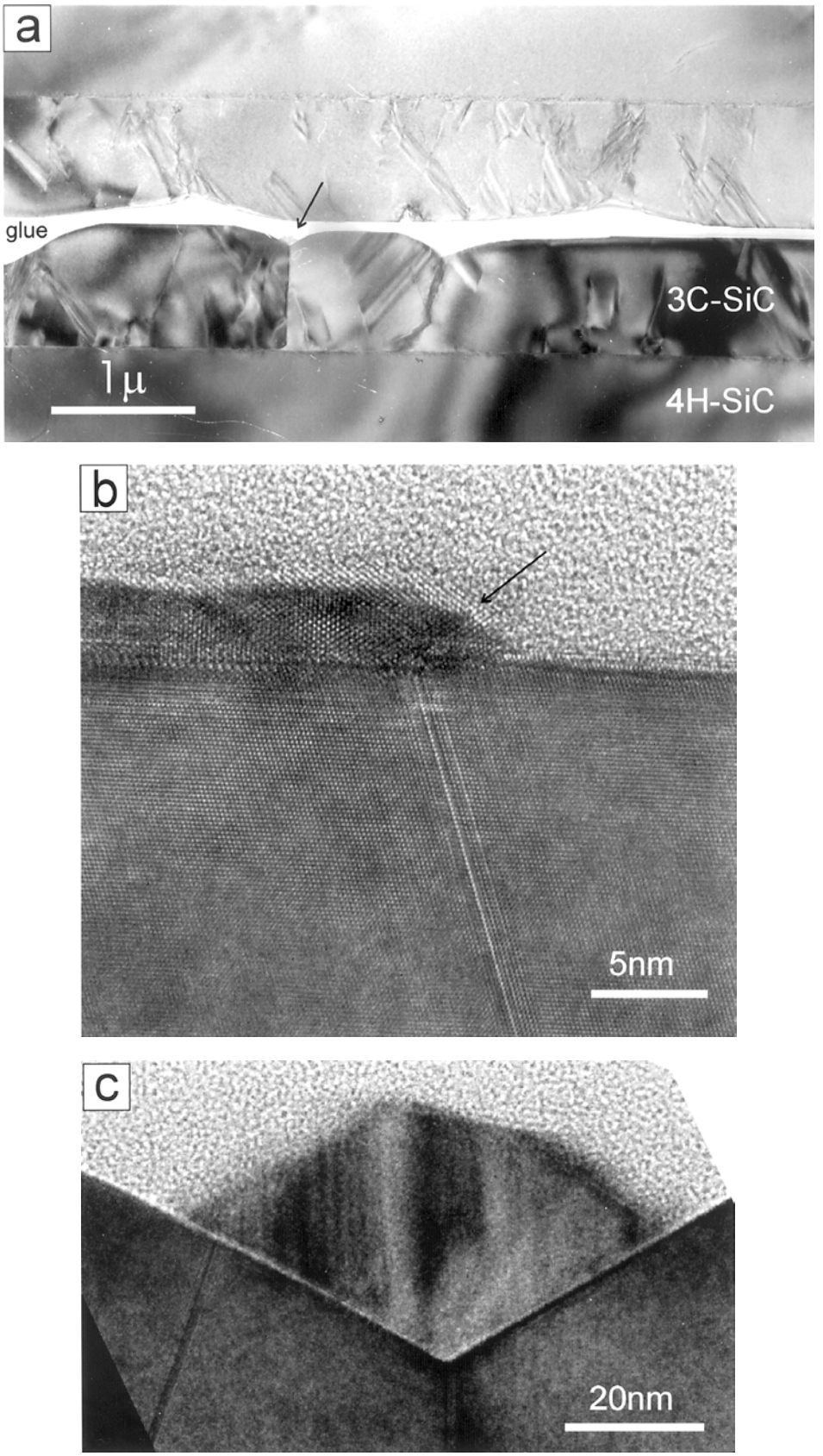

Fig. 1 (a) Low magnification bright-field image of a cubic SiC layer grown on 4H-SiC (at temperatures >900°C). The black arrow points to the big Si dot seen in (c) in higher magnification. Si nanocrystals form at the positions of stacking faults and growth facets, as shown in (b) and (c), respectively.

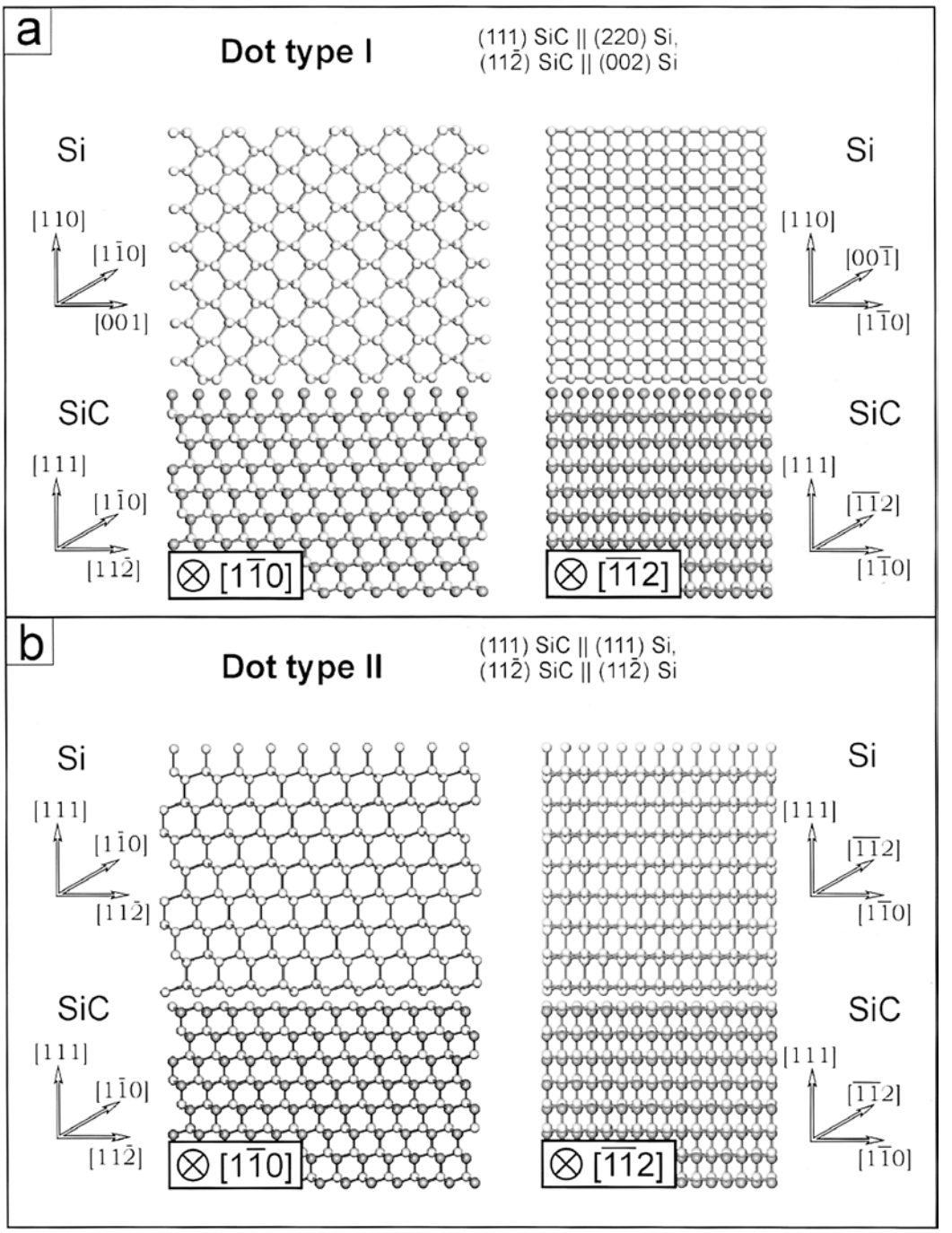

Fig. 2 (a) Dot type I and (b) dot type II orientation relationships observed experimentally.

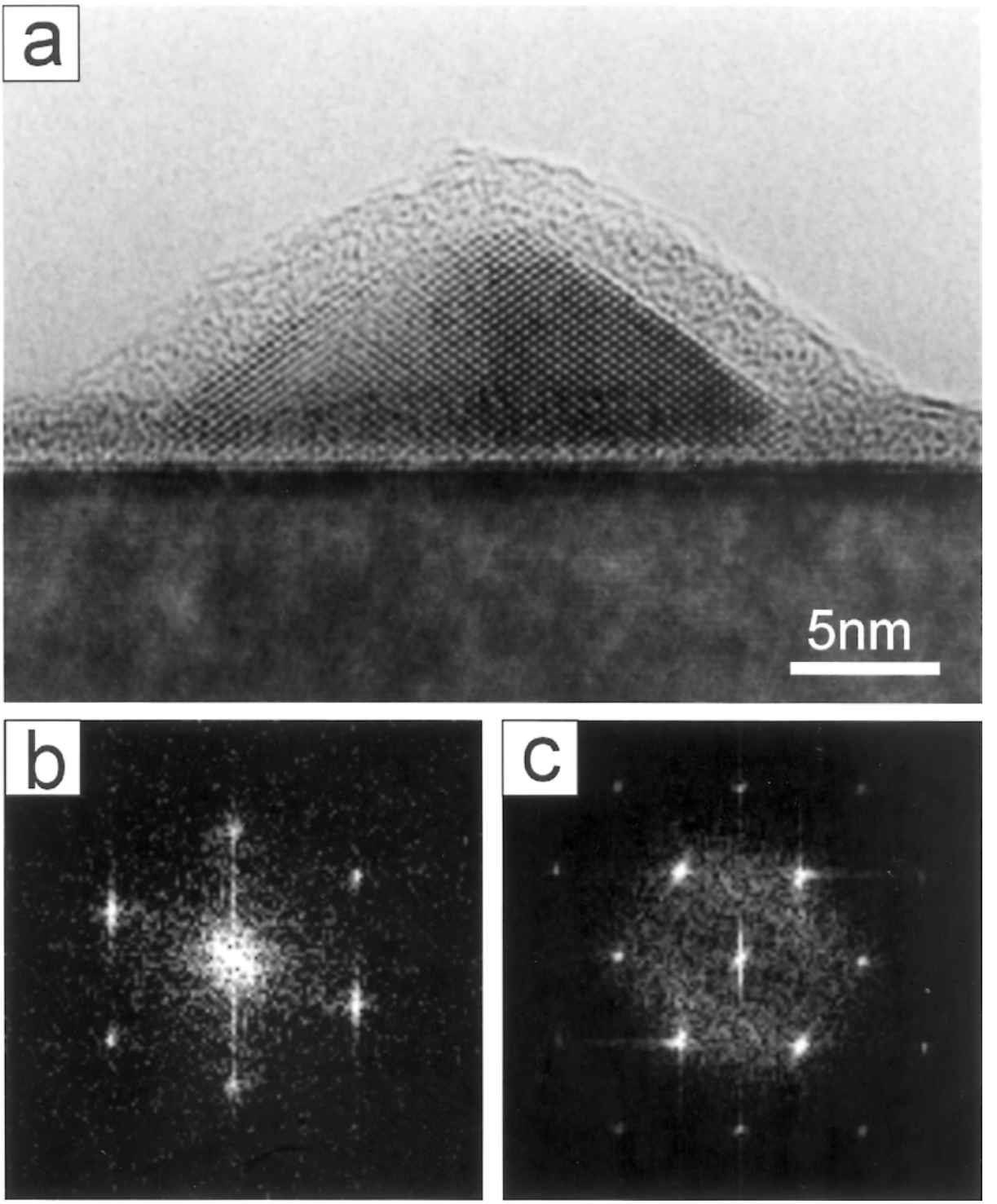

Fig. 3 (a) HRTEM image of a type I Si dot grown on 3C-SiC (at about 500°C substrate temperature), (b) Fourier transform from the 3C-SiC matrix, and (c) Fourier transform from the Si dot.

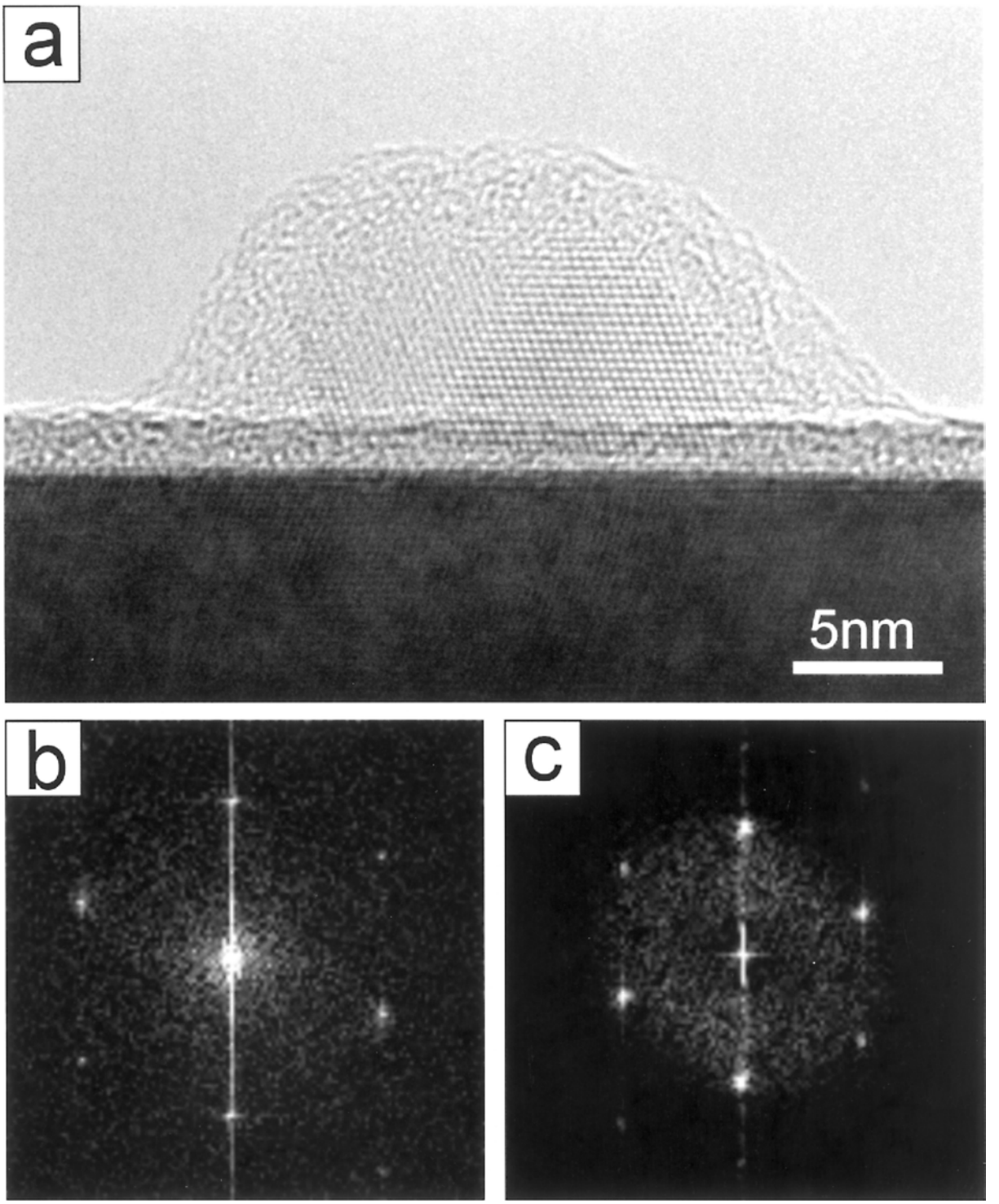

Fig. 4 (a) HRTEM image of the same specimen as presented in Fig. 3 showing a type II Si dot, (b) Fourier transform from the 3C-SiC matrix, and (c) Fourier transform from the Si dot.

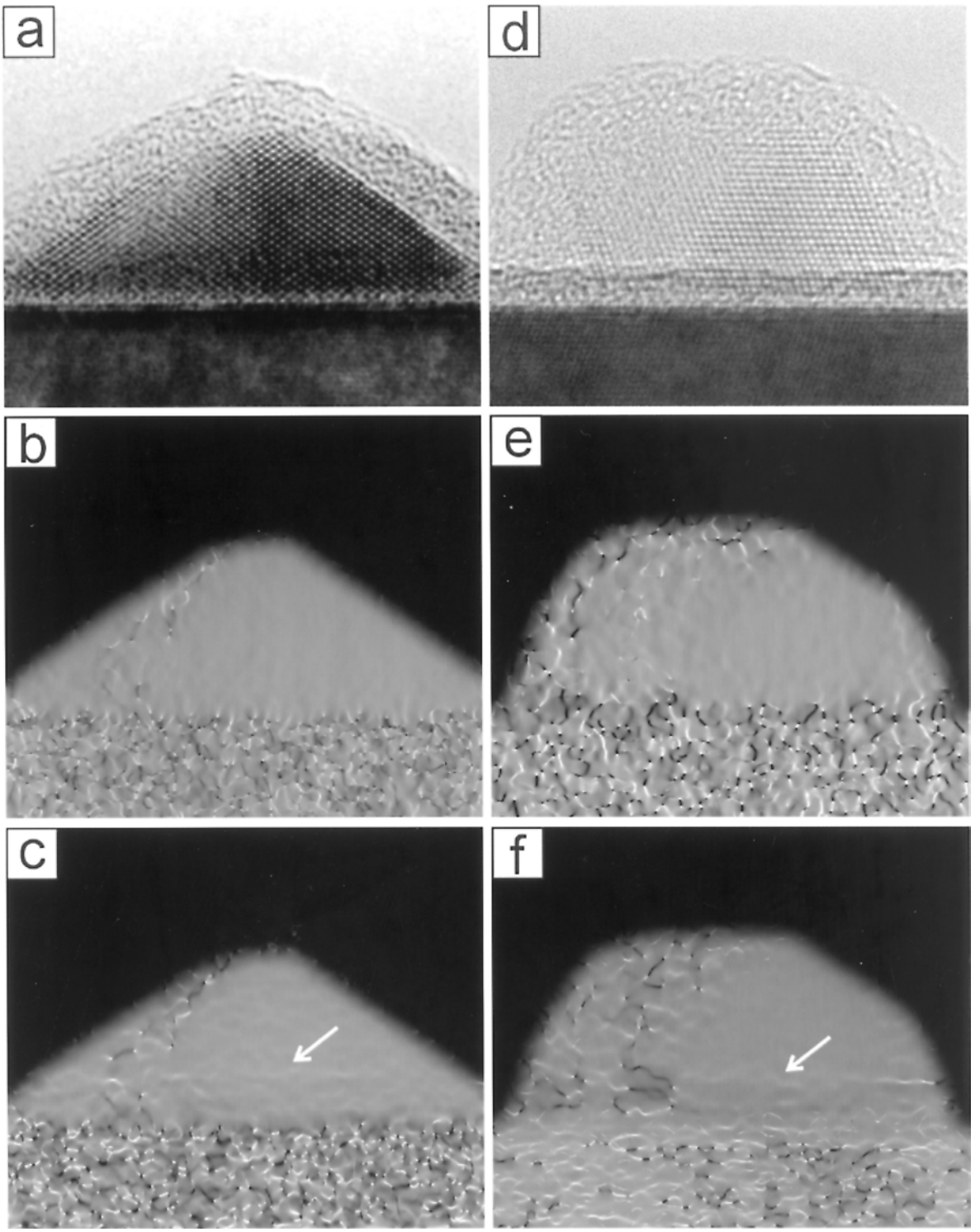

Fig. 5 Strain maps e_{xx} (b, e) and e_{yy} (c, f) obtained from HR images of type I and type II dots shown in (a) and (d). The white arrows in (c) and (f) point to contrast variations.

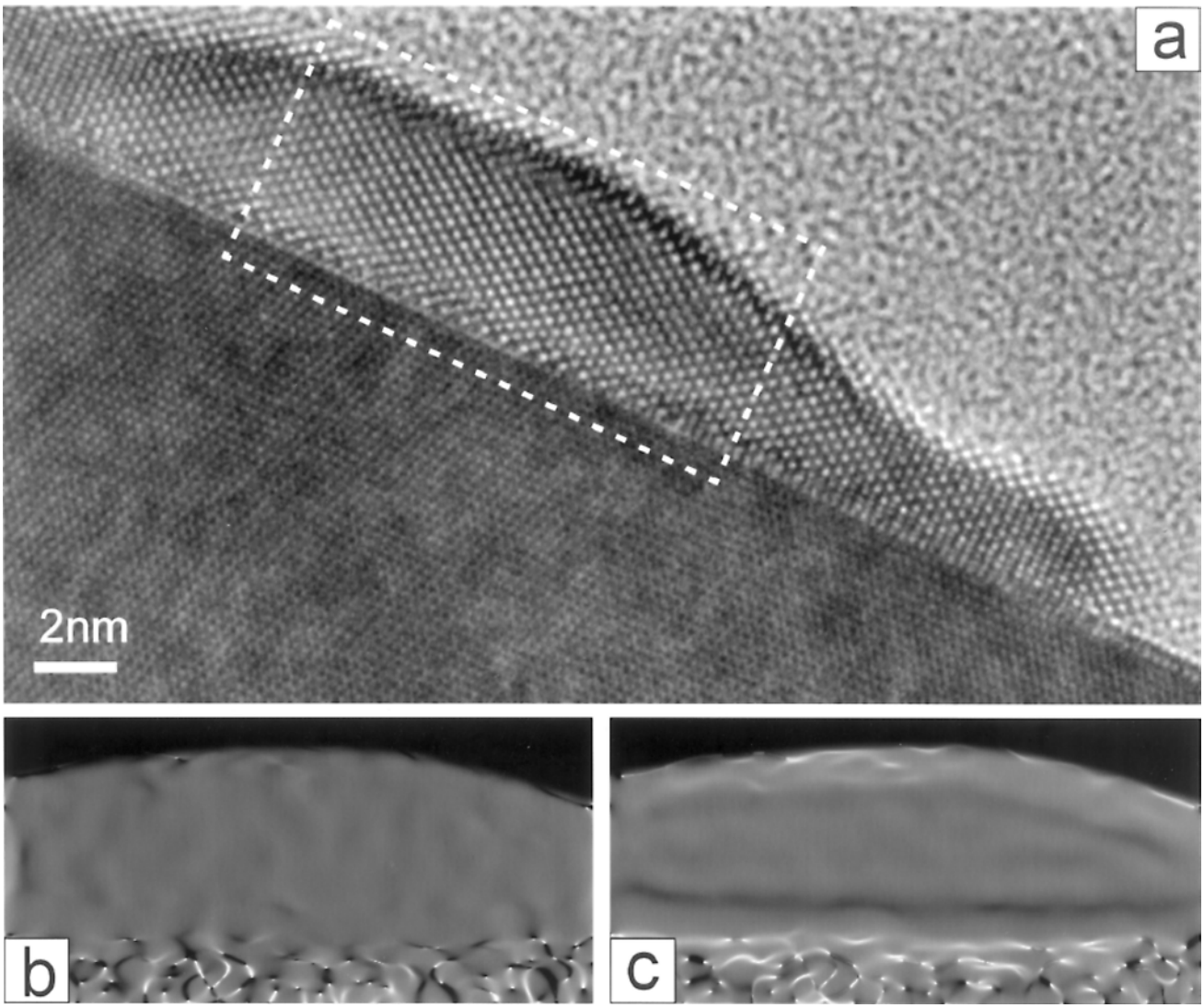

Fig. 6 (a) HRTEM image of a type I Si dot grown on 3C-SiC at a lower temperature. (b) and (c) Strain maps e_{xx} and e_{yy} determined from the area marked in (a).

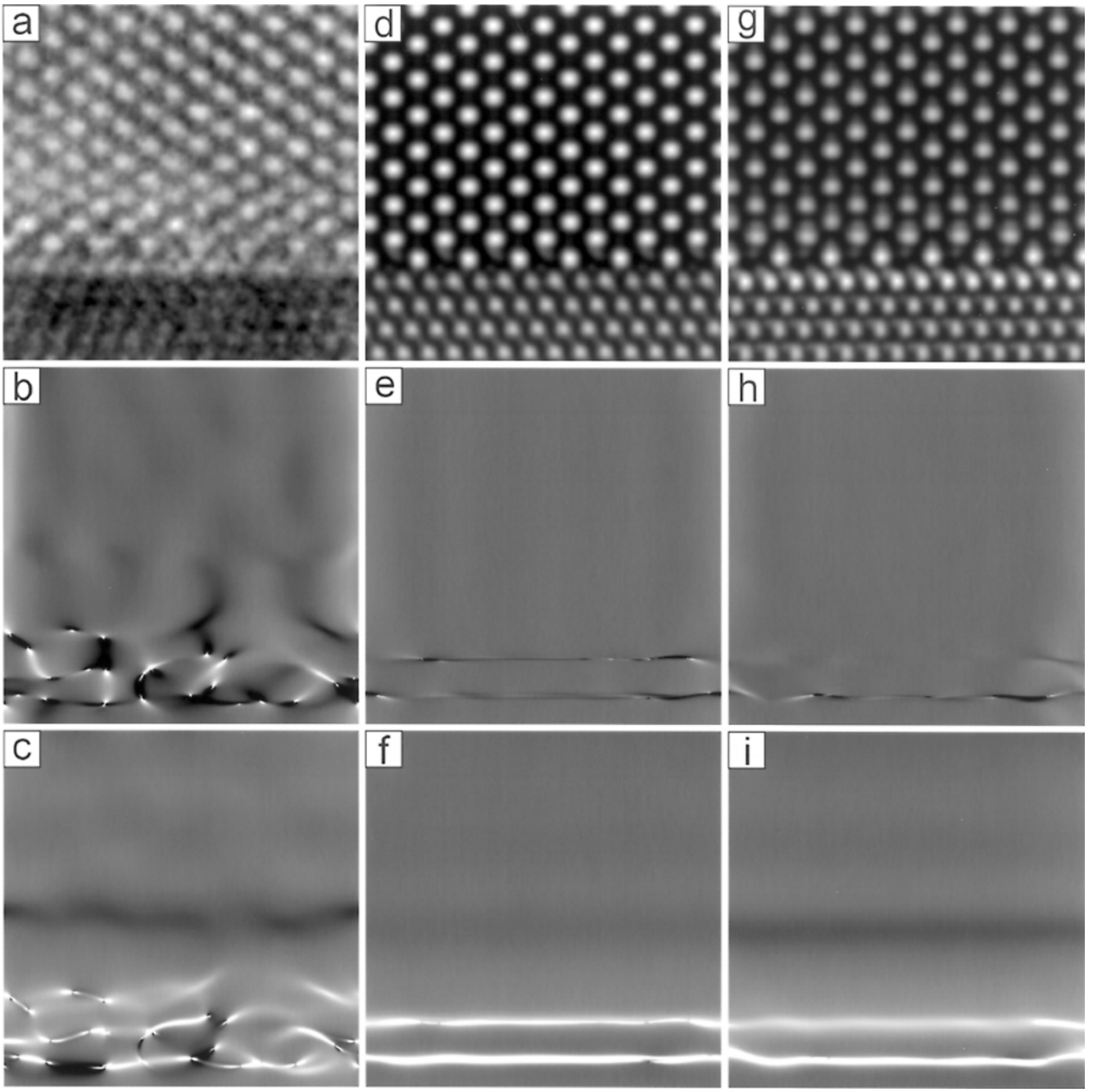

Fig. 7 Comparison of experimental data (a–c) taken from Fig. 6 with simulations (d–i). The corresponding plots of e_{xx} (b, e, h) and e_{yy} (c, f, i) are shown on the same intensity scale. (d) Calculated for a 250 Å thick Si dot grown on 450 Å of 3C-SiC (type I). (g) Contains an additional crystal tilt of 2 mrad (0.1°) towards the 111 (SiC) reflection. The latter model shows good qualitative agreement with the experimental data.